Modelling and multi-objective optimisation of the convective heat transfer characteristics and pressure drop of low concentration TiO_2-water nanofluids in the turbulent flow regime

M.Mehrabi, M.Sharifpur, J.P. Meyer*

Department of Mechanical and Aeronautical Engineering, University of Pretoria, Pretoria, Private Box X20, South Africa.

**Corresponding Author, e-mail: josua.meyer@up.ac.za*

Abstract

In the research for this paper, a GA-PNN hybrid system was used for modelling the convective heat transfer characteristics and pressure drop of TiO_2-water a nanofluid in a fully developed turbulent flow based on an experimentally obtained train and test data set. Models were developed for the Nusselt number and the pressure drop of the nanofluid as a function of Reynolds and Prandtl numbers, nanofluid volume concentration and average nanoparticle diameter. The results of the proposed models were compared with experimental data and with existing correlations. The validity of the proposed models was benchmarked by using statistical criteria and NSGA-II was used for multi-objective optimisation for the convective heat transfer. In the optimisation procedure model, the Nusselt number and pressure drop were considered as the objective functions. However, when the set of decision variables was selected based on the Pareto set, it ensures the best possible combination of objectives. The Pareto front of multi-objective optimisation of the Nusselt number and pressure drop proposed models were also shown and discussed. It was found that application of the multi-objective optimisation method for the turbulent convective heat transfer characteristics and pressure drop of TiO_2-water nanofluid could lead to finding the best design points based on the importance of the objective function in the design procedure.

Nomenclature

a_i	polynomial coefficient (weight)
d_p	nanoparticle average diameter, nm
f	friction factor
F	non-dominated front
L_{ij}	i-th output in j-th layer for the GA-PNN model
n	number of data points
N	population size
Nu	Nusselt number
ΔP	pressure drop, KPa
Pr	Prandtl number
Re	Reynolds number
X_p	predicted value
X_a	actual (experimental) data

Greek letters

ϕ	volume concentration, %

Subscripts

nf	nanofluid

Abbreviation

GA-PNN	genetic algorithm-polynomial neural network
GMDH	group method of data handling
NSGA-II	non-dominated sorting genetic algorithm II
MAE	mean absolute error
MRE	mean relative error
RMSE	root mean squared error

Keywords

TiO_2-water nanofluid; Nusselt number; pressure drop; genetic algorithm-polynomial neural network (GA-PNN); group method of data handling (GMDH); multi-objective optimisation; non-dominated sorting genetic algorithm II (NSGA-II)

1. Introduction

Due to the poor thermal properties of conventional heat transfer fluids, nanofluids as next-generation ones have recently received significant attention, especially after the Masuda et al. [1] and Choi [2] reports. Nanofluids are a class of heat transfer fluids which consist of a conventional base fluid with suspensions of low concentrations (usually up to 5% of volume fraction) of nanometer-sized particles (1-100 nm). These particles are generally metals, metal oxides or carbon nanotubes which are suspended in a base fluid such as water, engine oil, ethylene glycol (and/or mixture of them). More contact area between particles and fluids, high dispersion stability and reduced wearing and clogging are the main advantages of nanofluids in comparison with conventional solid-liquid suspensions [3]. Over the past two decades, the potential of the nanofluid as an ideal candidate for enhancing heat transfer in comparison with the conventional working fluids has been shown in the literature. Most of the previous works focused on potential applications, nanofluid synthesis, nanofluid physical properties and the heat transfer characteristics and pressure drop in a laminar or turbulent regime [4-13].

The most practical applications are in the turbulent flow regime, however, the investigation into the heat transfer and pressure drop for nanofluids in this regime and the optimisation of the heat transfer characteristics versus pressure drop are vital for improving the existing heating or cooling systems. It was found in the literature that by adding nanoparticles into the base fluid, the heat transfer characteristics would be enhanced. On the other hand the adding of nanoparticles increase the pressure drop, demanding more pumping power, which is not favourable at all. This is a multi-objective optimisation problem that should be solved to find the best design parameters to maximise the heat transfer characteristics and minimise the pressure drop.

Duangthongsuk and Wongwises [5] experimentally investigated the heat transfer performance and friction factor of TiO_2–water nanofluids for volume concentrations from 0.2% to 2% in the turbulent flow regime. Their experiments showed that the heat transfer coefficients for a 1% concentration of TiO_2–water nanofluid increased with 26% in comparison with the base fluid. It was also found that the pressure drop of nanofluid increased with the Reynolds number and was also greater than the pressure drop of the base fluid at the same Reynolds number.

Sajadi and Kazemi [6] investigated the convective heat transfer characteristics and friction factor of TiO_2–water nanofluid in a horizontal circular tube. They dispersed TiO_2 particles

with an average diameter of 30 nm into water and measured the Nusselt number and pressure drop of the nanofluid with volume concentrations up to 0.25% in a fully-developed turbulent regime. Their result showed that the addition of small amounts of nanoparticles to the base fluid augmented heat transfer significantly. For the pressure drop, they observed the same result as that of Duangthongsuk and Wongwises [5], namely that the pressure drop increased as the volume concentration increased and that the pressure drop was higher than that of the base fluid.

Abbasian Arani and Amani [13] reported experimental data for the convective heat transfer characteristics in fully developed turbulent flow of TiO_2–water nanofluids. The nanoparticles with average diameters of 10, 20, 30 and 50 were dispersed into the base fluid to investigate the effect of nanoparticle diameter on the Nusselt number and pressure drop of the nanofluid. Their experiments indicated that the nanofluid with a 20 nm nanoparticle size showed the best thermal performance in comparison with the others. Furthermore, they observed that adding nanoparticles did not have a significant effect on the nanofluid pressure drop compared with the base fluid.

During the last decade, there has been an interest in using soft computing methods which can transfer the knowledge and rules that exist beyond the empirical data into the network structure in order to use in applications. Recently, the application and capability of these methods, which are known as fuzzy logic, neural networks and genetic algorithms, to model and analyse engineering problems containing nanofluids have been increasingly developed. Santra et al. [14] predicted the average Nusselt number of the laminar natural convection of Cu-water nanofluid in a square cavity by using an artificial neural network which is trained by a resilient backpropagation algorithm. Hojjat et al. [15] modelled the thermal conductivity of γ-Al_2O_3, TiO_2 and CuO nanoparticles in a 0.5 wt% of carboxymethyl cellulose (CMC) aqueous solution by using a three-layer feedforward neural network. Papari et al. [16] modelled the thermal conductivity of single-wall carbon nanotubes and multi-wall carbon nanotubes dispersed into several base fluids by using a diffusion neural network. Longo et al. [17] presented two neural network models for predicting the thermal conductivity of Al_2O_3-water and TiO_2-water nanofluids by considering the volume fraction, temperature, nanoparticle diameter and particle thermal conductivity as the input variables. Mehrabi et al. [18] offered two models in order to model the thermal conductivity of alumina-water nanofluids by using a FCM-based neuro-fuzzy inference system as well as a genetic algorithm-polynomial neural network.

The engineering optimisation problems consist of multiple, often conflicting objectives that are supposed to be optimised simultaneously. The process of optimising a set of objective functions is called multi-objective optimisation (MOO) which has been widely used for more than two decades in real-world problems, especially in economics and engineering. In multi-objective optimisation problems there is a set of solutions (points) instead of a single optimised solution (point) in single-objective optimisation. All these points fit the Pareto optimality definition for an optimum result in a Pareto front [19].

Recently, there have been many investigations about using evolutionary algorithms (EAs) to develop the MOO approaches. This interest is due to the population-based search method, simplicity and finding the Pareto front in a single run. Genetic algorithms (GAs) are the most popular EAs for multi-objective design and optimisation problems. There are different multi-objective genetic algorithms (MOGAs) in the literature of which the differences are in the fitness assignment procedure, elitism or diversification approaches [20]. Among them, the non-dominated sorting genetic algorithm-II (NSGA-II) is one of the most efficient algorithms. The Pareto-based approach of NSGA-II has received significant attention after the first introduction by Deb et al. [21] to optimise a wide range of engineering problems [22-25]. In Section 6 of the present paper, this approach is described in detail.

In this paper, the Nusselt number and the pressure drop of TiO_2-water nanofluid were simulated by using the GA-PNN hybrid system approach and three experimental data sets [5, 6 and 13]. Next, the objective functions were used to obtain polynomial models for the effects of volume concentration, average particle diameter, Reynolds and Prandtl numbers on both the Nusselt number and the pressure drop. Finally, the obtained polynomial models were used in a Pareto-based multi-objective optimisation approach for finding the best possible combinations of the Nusselt number and pressure drop, known as the Pareto front.

2. Genetic algorithm-polynomial neural network hybrid system

In the research for the present paper, a GA-PNN hybrid system was applied for the simulation of the Nusselt number and pressure drop of TiO_2-water nanofluid in fully developed turbulent flow. The GA-PNN hybrid system was created by a combination of genetic algorithm and GMDH-type polynomial neural network approaches. In this hybrid system, a GMDH learning algorithm was used to instruct the polynomial neural network. The application of this learning algorithm to the polynomial neural network would introduce the GMDH-type polynomial neural network, which would be created for the neural network. On

the other hand, the genetic algorithm was used to find the hidden layers and bias coefficients of the GMDH-type polynomial neural network for minimising the training error and finding the optimal structure of the network. Detailed information about the GMDH-type polynomial neural network structure and GA-PNN hybrid system is given in Pesteei and Mehrabi [27] and Mehrabi et al. [18, 26], respectively.

3. Convective heat transfer of TiO_2-water nanofluid

Most of the fluid flow regimes are turbulent in industrial applications. Due to the presence of unsteady vortexes, the turbulent flow has more potential to enhance heat transfer. Therefore, the investigations into turbulent heat transfer of nanofluids are crucial for practical applications. Therefore, there are several studies in the literature on the convection heat transfer of TiO_2-water nanofluids in fully-developed turbulent flow regime [5, 6, 8, 12, 13 and 28].

In the present work, a new model was obtained by using the GA-PNN hybrid system as a function of the Reynolds number, Prandtl number, volume concentration and average particle size, which gives better accuracy for predicting the heat transfer performance of the TiO_2-water nanofluids. In the proposed model, the Nusselt number is related to the parameters as follows:

$$Nu_{nf} = f(Re, Pr, \phi, d_p) \tag{1}$$

The results of the proposed model were compared against experimental data [5, 6 and 13] as well as available correlations. The correlations, which were developed by Pak and Cho [29] (eq. 2) and Maiga et al. [30] (eq. 3), can predict the Nusselt number for the nanofluids in fully-developed turbulent flow.

$$Nu_{nf} = 0.021\, Re^{0.8} Pr^{0.5} \tag{2}$$

$$Nu_{nf} = 0.085\, Re^{0.71} Pr^{0.35} \tag{3}$$

The correlations determine the Nusselt numbers as a function of the Reynolds number and the Prandtl number.

Sajadi and Kazemi [6] proposed a correlation for the Nusselt number of TiO_2-water nanofluids in a fully developed turbulent regime as a function of the Reynolds number and the Prandtl number as:

$$Nu_{nf} = 0.067\, Re^{0.71} Pr^{0.35} + 0.0005\, Re \tag{4}$$

Duangthongsuk and Wongwises [5] and Abbasian Arani and Amani [28] offered correlations for the Nusselt number of TiO_2-water nanofluids as a function of the Reynolds number, the Prandtl number and volume concentration respectively, as follows:

$$Nu_{nf} = 0.074\, Re^{0.707} Pr^{0.385} \phi^{0.074} \quad (5)$$

$$Nu_{nf} = 0.041\, Re^{0.83} Pr^{1.35} (1 + \phi^{0.43}) \quad (6)$$

Unlike the present models for the Nusselt number, the dependence on the average particle diameter of the nanoparticles was not considered in these correlations.

4. Pressure drop of TiO_2-water nanofluid

For nanofluids to be used as next-generation heat transfer fluids in industrial applications, pressure drop information is also essential as it influences pumping power. In this paper, a new model was developed for the pressure drop of TiO_2-water nanofluids in fully-developed turbulent flow by using a GA-PNN hybrid system as a function of Reynolds number, volume concentration and average particle size. In the model, the pressure drop is a function of Reynolds number, nanoparticle volume concentration and the diameter of nanoparticles, thus:

$$\Delta P_{nf} = f(Re, \phi, d_p) \quad (7)$$

5. Predictive ability of the models

A total of 168 input-output experimental data points obtained from literature [5, 6 and 13] were used in order to predict the Nusselt number for a TiO_2-water nanofluid. The experimental data were divided into two subsets as 75% (127 data points) for training and 25% (41 data points) for testing purposes. In order to model the pressure drop 151 experimental data points from [5, 6 and 13] were divided to subsets as 81% (124 data points) for training and 19% (29 data points) for testing purposes.

The mean absolute error (*MAE*), mean relative error (*MRE*) and root mean square errors (*RMSE*) criteria were used as given in Table 1. It shows the accuracy of the GA-PNN models in order to predict the Nusselt number and pressure drop of TiO_2-water nanofluid for various values of inlet variables.

5.1. Nusselt number prediction

The structure of the GA-PNN model for predicting the Nusselt number of TiO_2-water nanofluid is shown in Fig. 1, and corresponds to the genome representation of ***3312141411342222,*** in which ***1, 2, 3*** and ***4*** stand for volume concentration ϕ (%), average

particle diameter d_p (nm) , the Reynolds number *Re* and the Prandtl number *Pr* respectively. The corresponding polynomial representation of the model for the Nusselt number of TiO_2-water nanofluid is shown in Appendix I.

5.1. Pressure drop prediction

The structure of the GA-PNN model for prediction the pressure drop of TiO_2-water nanofluid is shown in Fig. 2 corresponding to the genome representation of ***1211221333122323,*** in which ***1, 2*** and ***3*** stand for volume concentration ϕ (%), average particle diameter d_p (nm) and the Reynolds number *Re*, respectively. The corresponding polynomial representation of the model for the pressure drop of TiO_2-water nanofluid is shown in the appendix II.

6. Multi-objective optimisation by using NSGA-II

In most real-engineering problems, a unique solution based on the single-objective optimisation techniques is unable to present an acceptable result for the other objective functions, especially when there is more than one objective function that may be in conflict with one another. Multi-objective optimisation is defined as a technique that gives a reasonable set of solutions for all objective functions by finding the vector of decision variables, when the constraints are satisfied. This set of solutions satisfies the objective functions at an acceptable level without being dominated by other sets. This set of non-dominated solutions is called the Pareto optimal set. The corresponding objective function value for a given Pareto optimal set is referred to as the Pareto front.

Various multi-objective algorithms have been applied for solving engineering problems in the last two decades [20, 31-37], among them the non-dominated sorting genetic algorithm II (NSGA-II), which was chosen for this investigation.

There are different operators for the NSGA-II algorithm including initialisation, evaluation, fast non-dominated sorting, crowding distance assignment, selection, crossover and mutation. The procedure and flow diagram of this algorithm are shown below:

NSGA II Algorithm

Step 1: generate a parent population P_0 of size *N*, randomly
Step 2: set $t = 0$
Step 3: create offspring population Q_0 of size *N*, by application of crossover and mutation to P_0
Step 4: if the stop criterion is satisfied, stop and return P_t
Step 5: set $R_t = P_t \cup Q_t$
Step 6: set $F = (F_1, F_2, \dots, F_K) =$ fast-non-dominated-sort (R_t)
Step 7: for $i = 1{:}\,k$ do the following substeps:
    7.1: calculate the crowding-distance-assignment (F_i)
    7.2: set P_{t+1} as follows:
        if $|P_{t+1}| + |F_i| \leq N$;
        $P_{t+1} = P_{t+1} \cup F_i$
        then ($|P_{t+1}| + |F_i| > N$);
        $P_{t+1} = P_{t+1} \cup F_i[1{:}\,(N - |P_{t+1}|)]$
Step 8: this step consists of the following two substeps:
    8.1: select parent from P_{t+1} by using binary tournament selection on the crowding distance
    8.2: create offspring population Q_{t+1} of size *N*, by application of crossover & mutation to P_{t+1}
Step 9: set $t = t + 1$ and go to the fourth step

The NSGA-II uses a fast non-dominated sorting operator for fitness assignments. In the process of fitness assignment, the solution set not dominated by any other solutions in the population is assigned as the first front and given the highest fitness value; the solution set dominated by solutions in the first front is assigned as the second front and given the second-highest fitness value. This procedure will iterate until all the solution sets are given a fitness value. The crowding distance is the normalised distance between a solution vector and its closest neighbouring solution vector in each of the fronts.

The selection is achieved in binary tournament of two solution vectors. The solution vector with the lowest front number is selected if the two solution vectors are from different fronts. If both the solution vectors are on the same front, then the solution with the highest crowding distance is selected.

In the NSGA-II algorithm, simulated binary crossover (SBX) and highly disruptive polynomial mutation approaches are used for crossover and mutation operators. The SBX applies to two parent solutions and creates two offsprings. The difference between an offspring and parent depends on the crossover index, which is a non-negative real number. A large value of the crossover index gives a higher probability for creating 'near-parent' solutions and a small value of it allows distant solutions to be selected as an offspring. The application of highly disruptive polynomial mutation gives the system the possibility of doing larger jumps in the search space and avoiding the local optimal points [38].

The detailed information about the NSGA-II Algorithm, fast non-dominated sorting operator, crowding-distance-assignment operator, selection method and simulated binary crossover (SBX) operator are fully described in Refs [21 and 38].

The conflicting objectives in this study are the Nusselt number and pressure drop that are optimised with respect to the volume concentration ϕ, average particle diameter d_p, the Reynolds number *Re* and the Prandtl number *Pr*, which are called design variables. In this two-objective optimisation problem, the goal is finding the best design variable value in order to maximise the Nusselt number and minimise the pressure drop simultaneously.

7. Results and discussion

Fig. 3 shows the experimental results of Sajadi and Kazemi [6] compared with the GA-PNN model for the Nusselt number of TiO_2-water nanofluid and also correlations with a particle size of 30 nm, volume concentration of 0.1% at various Reynolds numbers ranging from 6 000 to 30 000. The model for Nusselt number is in very good agreement with the experimental data (*MAE* = 3.7, *MRE* = 3.5% and *RMSE* = 4.4). The proposed GA-PNN model is well matched with the experimental data and predicts the Nusselt number better than all correlations [5, 28, 29 and 30].

Fig. 4 shows the experimental results of Duangthongsuk and Wongwises [5] compared with the GA-PNN model. Also, the correlations from literature for a particle size of 21 nm and volume concentration of 1% for a TiO_2-water nanofluid over a Reynolds number range from 4 500 to 14 500. The GA-PNN model is in good agreement with the experimental data (*MAE* = 3.4, *MRE* = 3.7% and *RMSE* = 3.6), and the GA-PNN proposed model and Sajadi and Kazemi [6] correlation predict the Nusselt number better than other correlations [28, 29 and 30].

Fig. 5 shows the experimental results of Abbasian Arani and Amani [13] compared with the GA-PNN model. Also, the correlations from literature for a particle size of 50 nm and volume concentration of 1% for a TiO2-water nanofluid. The GA-PNN model is in great agreement with the experimental data (MAE = 5.9, MRE = 2.7% and RMSE = 6.9), and the GA-PNN proposed model and Maiga et al. [30] correlation predict the Nusselt number better than other correlations.

In Figs. 6 and 7, the experimental results of Abbasian Arani and Amani [13] are compared with those of the GA-PNN model and the correlations for the Nusselt number of TiO_2-water nanofluid with particle sizes of 10 nm and 20 nm, and volume concentration of 1.5% and 2%, respectively. Based on the result of Fig.6 the GA-PNN model is well matched with the

experimental data in comparison with the correlations (*MAE* = 5.6, *MRE* = 4.8% and *RMSE* = 8.1), especially in the high Reynolds number range from 20 000 – 44 000. Fig.7 shows that the GA-PNN model is in a good agreement with the experimental data (*MAE* = 20.3, *MRE* = 8.1% and *RMSE* = 21.3) and predicts the Nusselt number the best while the existing correlations significantly under-predicted the experimental data.

Considering figures 6 and 7, it can be concluded that for TiO_2-water nanofluids with increase in Reynolds number as well as volume concentration the exciting correlations are unable to predict the Nusselt number properly and the GA-PNN model predicts the Nusselt number better than those of the correlations in literature in all cases.

Fig. 8a shows a comparison between the experimental results of Sajadi and Kazemi [6] and the GA-PNN model for the pressure drop of a TiO_2-water nanofluid with a particle size of 30 nm, volume concentration of 0.15% and Reynolds number ranging from 6 000 to 30 000. The GA-PNN model (*MAE* = 0.47, *MRE* = 5.0% and *RMSE* = 0.53) corresponds very well with the experimental data.

In Fig. 8b, the experimental results of Duangthongsuk and Wongwises [5] are compared with those of the GA-PNN model and the correlations for the pressure drop of TiO_2-water nanofluid with a particle size of 21 nm, and a volume concentration of 1.5% and Reynolds number ranging from 4 500 to 14 500. The GA-PNN model predicts the pressure drop the best when compared with the measurements (*MAE* = 0.12, *MRE* = 2.0% and *RMSE* = 0.21).

Fig. 8c shows the experimental results of Abbasian Arani and Amani [13] compared with the GA-PNN model for a particle size of 30 nm and volume concentration of 1%. The GA-PNN model is not in such a good agreement with the experimental data and the (*MAE* = 3.9, *MRE* = 54.4% and *RMSE* = 3.9). Although the proposed model is not well matched with the experimental data, the model trend is the same as experimental data and because the proposed model over-predicted the experimental data, it might give us more conservative result points in the optimisation part.

In Fig. 8d, the experimental result of Abbasian Arani and Amani [13] is compared with those of the GA-PNN model for a particle size of 50 nm and volume concentration of 1.5%. The GA-PNN model matches the data very well (*MAE* = 0.835, *MRE* = 8.9% and *RMSE* = 1.01).

Fig. 9 shows the Pareto front of the Nusselt number and pressure drop. By choosing the appropriate value for one objective function may cause a poor value for the second objective function. In this Pareto front, all the points (Pareto sets) are optimum points based on the

multi-objective optimisation concepts and the final design point should be chosen by the designer based on the importance of each objective function in the design procedure. In this Pareto front, the optimal design points are divided into three sections and the corresponding design variables (input variables) as well as objective functions for the six optimal points, which are shown in Table 2 (they are related to start and end points). In Section I, which is started at point A and ends at B, the Nusselt number increases by 45% (from 64.23 to 91.11) when the pressure drop increases by 14% (from 2.42 to 2.75). In Section II which starts at point C and ends at D, there is a direct relationship between the increase in the pressure drop and increase in Nusselt number. In this section, the pressure drop increases by 271% when the Nusselt number increases by 179%. It is obvious that the design points in Section III should not be chosen as the best design points, because of the 19% increase in the pressure drop; while there is no significant increase in the Nusselt number from Point E to Point F. So, choosing the final design points from Section II is a better choice in comparison with the other sections. However, it is important to notice that all the points in this Pareto front are optimal points and the designer could choose any of these optimal points for the best design point. It is related to the importance of objective functions in the design procedure.

8. Conclusions

In the present study, the GA-PNN hybrid system was used for modelling the convective heat transfer characteristics and pressure drop of TiO_2-water nanofluid in fully developed turbulent flow based on an input-output experimental data set as function of the Reynolds number, the Prandtl number, nanoparticle volume concentration and average nanoparticle diameter. In the GA-PNN hybrid system, consisting of a neural network and genetic algorithm part, the genetic algorithm was used to find the best network weights for minimising the training error and finding the optimal structure for a GMDH-type polynomial neural network. In the neural network part of this hybrid system, the group method of data handling (GMDH) learning approach was used to learn a second-rate polynomial neural network. The structure of the proposed models based on the genome representation for the Nusselt number as well as pressure drop with respect to effective (input) parameters has been developed. The results of the models were compared with the experimental data points and with existing correlations from literature. The statistical error analysis shows that the proposed models are in good agreement compared with experimental data and shows better accuracy with experimental data in comparison with the existing correlations.

The proposed models for the Nusselt number and pressure drop were used in a multi-objective optimisation problem based on the NSGA-II algorithm. The Pareto front of these two conflicting objective functions was shown and discussed. The combination of the GA-PNN hybrid system for the modelling part and the use of the NSGA-II algorithm for multi-objective optimisation for turbulent convection heat transfer of TiO_2-water nanofluids showed very interesting results.

Acknowledgements

The funding obtained from the NRF, Stellenbosch University/University of Pretoria Solar Hub, CSIR, EEDSM Hub, RDP and NAC is acknowledged and duly appreciated.

Appendix I:

$$L_{11} = a_{1,0} + a_{1,1}.\phi + a_{1,2}.d_p + a_{1,3}.\phi.d_p + a_{1,4}.\phi^2 + a_{1,5}.{d_p}^2$$

$$L_{21} = a_{2,0} + a_{2,1}.\phi + a_{2,2}.Pr + a_{2,3}.\phi.Pr + a_{2,4}.\phi^2 + a_{2,5}.Rr^2$$

$$L_{31} = a_{3,0} + a_{3,1}.Re + a_{3,2}.Pr + a_{3,3}.Re.Pr + a_{3,4}.Re^2 + a_{3,5}.Pr^2$$

$$L_{12} = a_{4,0} + a_{4,1}.Re + a_{4,2}.L_{11} + a_{4,3}.Re.L_{11} + a_{4,4}.Re^2 + a_{4,5}.{L_{11}}^2$$

$$L_{22} = a_{5,0} + a_{5,1}.\phi + a_{5,2}.L_{31} + a_{5,3}.\phi.L_{31} + a_{5,4}.\phi^2 + a_{5,5}.{L_{31}}^2$$

$$L_{13} = a_{6,0} + a_{6,1}.L_{12} + a_{6,2}.L_{21} + a_{6,3}.L_{12}.L_{21} + a_{6,4}.{L_{12}}^2 + a_{6,5}.{L_{21}}^2$$

$$L_{23} = a_{7,0} + a_{7,1}.L_{22} + a_{7,2}.d_p + a_{7,3}.L_{22}.d_p + a_{7,4}.{L_{22}}^2 + a_{7,5}.{d_p}^2$$

$$Nu_{nf} = a_{8,0} + a_{8,1}.L_{13} + a_{8,2}.L_{23} + a_{8,3}.L_{13}.L_{23} + a_{8,4}.{L_{13}}^2 + a_{8,5}.{L_{23}}^2$$

$$[\mathbf{a}_{ij}] = \begin{bmatrix} 67.39861967 & 155.3890385 & -0.54661578 & -67.4937622 & 0.006683105 & 1.25041801 \\ -625.276506 & 5.001759885 & 467.1605151 & 54.2212255 & -58.2092747 & -42.824571 \\ 2.197 \times 10^{-7} & 0.002868903 & 2.308 \times 10^{-7} & -2.92 \times 10^{-8} & -7.15 \times 10^{-7} & 0.00177207 \\ 4.509 \times 10^{-7} & 0.005725457 & 3.199 \times 10^{-5} & -1.44 \times 10^{-8} & 0.000360089 & 1.292 \times 10^{-5} \\ 12.62326281 & -28.6139037 & 0.792949239 & 12.08935958 & -0.00018628 & 0.194649498 \\ 50.15011252 & 0.442351847 & -0.56421161 & -0.00034801 & 0.001662117 & 0.003198651 \\ -9.63382038 & 1.031554882 & 0.624331389 & 0.000229741 & -0.00289168 & -0.00401269 \\ -2.18155351 & 0.533902305 & 0.507308577 & -0.00521318 & -0.00314481 & 0.008270173 \end{bmatrix}$$

Appendix II:

$$L_{11} = a_{1,0} + a_{1,1}.\phi + a_{1,2}.d_p + a_{1,3}.\phi.d_p + a_{1,4}.\phi^2 + a_{1,5}.{d_p}^2$$

$$L_{21} = a_{2,0} + a_{2,1}.\phi + a_{2,2}.Re + a_{2,3}.\phi.Re + a_{2,4}.\phi^2 + a_{2,5}.Re^2$$

$$L_{31} = a_{3,0} + a_{3,1}.d_p + a_{3,2}.Re + a_{3,3}.d_p.Re + a_{3,4}.{d_p}^2 + a_{3,5}.Re^2$$

$$L_{12} = a_{4,0} + a_{4,1}.L_{11} + a_{4,2}.\phi + a_{4,3}.L_{11}.\phi + a_{4,4}.{L_{11}}^2 + a_{4,5}.\phi^2$$

$$L_{22} = a_{5,0} + a_{5,1}.d_p + a_{5,2}.L_{21} + a_{5,3}.d_p.L_{21} + a_{5,4}.{d_p}^2 + a_{5,5}.{L_{21}}^2$$

$$L_{32} = a_{6,0} + a_{6,1}.L_{11} + a_{6,2}.Re + a_{6,3}.L_{11}.Re + a_{6,4}.{L_{11}}^2 + a_{6,5}.Re^2$$

$$L_{13} = a_{7,0} + a_{7,1}.L_{12} + a_{7,2}.L_{22} + a_{7,3}.L_{12}.L_{22} + a_{7,4}.{L_{12}}^2 + a_{7,5}.{L_{22}}^2$$

$$L_{23} = a_{8,0} + a_{8,1}.L_{32} + a_{8,2}.L_{31} + a_{8,3}.L_{32}.L_{31} + a_{8,4}.{L_{32}}^2 + a_{8,5}.{L_{31}}^2$$

$$\Delta P_{nf} = a_{9,0} + a_{9,1}.L_{13} + a_{9,2}.L_{23} + a_{9,3}.L_{13}.L_{23} + a_{9,4}.{L_{13}}^2 + a_{9,5}.{L_{23}}^2$$

$$[\mathbf{a}_{ij}] = \begin{bmatrix} -4.901 \times 10^{-7} & -2.521 \times 10^{-5} & 0.00040705 & -0.0013582 & 1.415 \times 10^{-9} & 1.994 \times 10^{-6} \\ 4.346 \times 10^{-8} & 2.525 \times 10^{-8} & 0.00045035 & 2.638 \times 10^{-8} & 3.889 \times 10^{-9} & -8.86 \times 10^{-5} \\ 7.78933893 & 2.341589898 & -0.2035313 & 2.66252775 & 0.109419333 & -0.31805789 \\ 5.39159929 & -11.5340018 & 0.86942588 & 4.75545983 & 0.013934046 & -0.09116812 \\ -31.694717 & 16.11679573 & 6.16097472 & -1.9169856 & -0.19310173 & -1.30663773 \\ -6.4420171 & 1.178165895 & 0.43875907 & -0.0061312 & -0.00702419 & -0.00039369 \\ 0.31629638 & 0.318197046 & 0.65454924 & -0.0766096 & -0.15295112 & 0.231249939 \\ 1.53695886 & -0.00558705 & 0.37241296 & -0.0113919 & 0.008688029 & 0.047656331 \\ -0.1436674 & 0.770220048 & 0.27359825 & -0.0298951 & -0.04116522 & 0.069972926 \end{bmatrix}$$

References

[1] H. Masuda, A. Ebata, K. Teramae, N. Hishinuma, Alteration of thermal conductivity and viscosity of liquid by dispersing ultra-fine particles (dispersion of c-Al_2O_3, SiO_2 and TiO_2 ultra-fine particles), Netsu Bussei 4 (1993) 227–233.

[2] S.U.S. Choi, Enhancing thermal conductivity of fluids with nanoparticles. ASME FED 231 (1995) 99–103.

[3] R. Saidur, K.Y. Leong, H.A. Mohammad, A review on applications and challenges of nanofluids, Renew. Sust. Energ. Rev.15 (2011) 1646–1668.

[4] X. Wei, H. Zhu, T. Kong, L. Wang, Synthesis and thermal conductivity of Cu_2O nanofluids, Int. J. Heat Mass Transfer 52 (2009) 4371–4374.

[5] W. Duangthongsuk, S. Wongwises, An experimental study on the heat transfer performance and pressure drop of TiO_2-water nanofluids flowing under a turbulent flow regime, Int. J. Heat Mass Transfer 53 (2010) 334–344.

[6] A.R. Sajadi, M.H. Kazemi, Investigation of turbulent convective heat transfer and pressure drop of TiO_2/water nanofluid in circular tube, Int. Commun. Heat Mass 38 (2011) 1474–1478.

[7] G. Paul, J. Philip, B. Raj, P. K. Das, I. Manna, Synthesis, characterization, and thermal property measurement of nano-$Al_{95}Zn_{05}$ dispersed nanofluid prepared by a two-step process, Int. J. Heat Mass Transfer 54 (2011) 3783–3788.

[8] L. Godson, B. Raja, D. Mohan Lal, S. Wongwises, Convective heat transfer characteristics of silver-water nanofluid under laminar and turbulent flow conditions, J. Thermal Sci. Eng. Appl. 4(3) (2012) 031001.

[9] A. Nasiri, M. Shariaty-Niasar, A.M. Rashidi, R. Khodafarin, Effect of CNT structures on thermal conductivity and stability of nanofluid, Int. J. Heat Mass Transfer 55 (2012) 1529–1535.

[10] A.T. Utomo, H. Poth, P.T. Robbins, A.W. Pacek, Experimental and theoretical studies of thermal conductivity, viscosity and heat transfer coefficient of titania and alumina nanofluids, Int. J. Heat Mass Transfer 55 (2012) 7772–7781.

[11] M.M. Heyhat, F. Kowsary, A.M. Rashidi, S. Alem Varzane Esfehani, A. Amrollahi, Experimental investigation of turbulent flow and convective heat transfer characteristics of alumina water nanofluids in fully developed flow regime, Int. Commun. Heat Mass 39 (2012) 1272–1278.

[12] M. Keshavarz Moraveji, M. Hejazian, Modeling of turbulent forced convective heat transfer and friction factor in a tube for Fe_3O_4 magnetic nanofluid with computational fluid dynamics, Int. Commun. Heat Mass 39 (2012) 1293–1296.

[13] A.A. Abbasian Arani, J. Amani, Experimental investigation of diameter effect on heat transfer performance and pressure drop of TiO_2–water nanofluid, Exp. Therm. Fluid Sci. 44 (2013) 520–533.

[14] A.K. Santra, N. Chakraborty, S. Sen, Prediction of heat transfer due to presence of copper–water nanofluid using resilient-propagation neural network, Int. J. Therm. Sci. 48 (2009) 1311–1318.

[15] M. Hojjat, S.Gh. Etemad, R. Bagheri, J. Thibault, Thermal conductivity of non-Newtonian nanofluids: Experimental data and modeling using neural network, Int. J. Heat Mass Transfer 54 (2011) 1017–1023.

[16] M.M. Papari, F.Yousefi, J. Moghadasi, H. Karimi, A. Campo, Modeling thermal conductivity augmentation of nanofluids using diffusion neural networks, Int. J. Therm. Sci. 50 (2011) 44-52.

[17] G.A. Longo, C. Zilio, E. Ceseracciu, M. Reggiani, Application of Artificial Neural Network (ANN) for the prediction of thermal conductivity of oxide–water nanofluids, Nano Energy 1 (2012) 290–296.

[18] M. Mehrabi, M. Sharifpur, J.P. Meyer, Application of the FCM-based neuro-fuzzy inference system and genetic algorithm-polynomial neural network approaches to modelling the thermal conductivity of alumina–water nanofluids, Int. Commun. Heat Mass 39 (2012) 971–977.

[19] V. Pareto, Cours d'economic politique, Rouge, Lausanne, Switzerland (1896)

[20] R.T. Marler, J.S. Arora, Survey of multi-objective optimization methods for engineering, Struct. Multidiscip. O. 26 (2004) 369–395.

[21] K. Deb, A. Pratap, S. Agarwal, T. Meyarivan, A fast and elitist multiobjective genetic algorithm: NSGA-II, IEEE T. Evolut. Comput. 6(2) (2002) 182–197.

[22] K. Foli, T. Okabe, M. Olhofer, Y. Jin, B. Sendhoff, Optimization of micro heat exchanger: CFD, analytical approach and multi-objective evolutionary algorithms, Int. J. Heat Mass Transfer 49 (2006) 1090–1099.

[23] D. Copiello, G. Fabbri, Multi-objective genetic optimization of the heat transfer from longitudinal wavy fins, Int. J. Heat Mass Transfer 52 (2009) 1167–1176.

[24] A. Husain, K.Y. Kim, Analysis and optimization of electrokinetic microchannel heat sink, Int. J. Heat Mass Transfer 52 (2009) 5271–5275.

[25] A. Lemouedda, M. Breuer, E. Franz, T. Botsch, A. Delgado, Optimization of the angle of attack of delta-winglet vortex generators in a plate-fin-and-tube heat exchanger, Int. J. Heat Mass Transfer 53 (2010) 5386–5399.

[26] M. Mehrabi, S. Rezazadeh, M. Sharifpur, J.P. Meyer, Modeling of proton exchange membrane fuel cell (PEMFC) performance by using genetic algorithm-polynomial neural network (GA-PNN) hybrid system. Proceedings of the ASME 2012 10th Fuel Cell Science, Engineering and Technology Conference (FuelCell2012), San Diego, USA, 2012, paper FuelCell2012-91391.

[27] S.M. Pesteei, M. Mehrabi, Modeling of convection heat transfer of supercritical carbon dioxide in a vertical tube at low Reynolds numbers using artificial neural network, International Communications in Heat and Mass Transfer 37 (2010) 901–906.

[28] A.A. Abbasian Arani, J. Amani, Experimental study on the effect of TiO_2–water nanofluid on heat transfer and pressure drop, Exp. Therm. Fluid Sci. 42 (2012) 107–115.

[29] B.C. Pak, Y.I. Cho, Hydrodynamic and heat transfer study of dispersed fluids with submicron metallic oxide particles, Exp. Heat Transfer 11(2) (1998) 151–170.

[30] S.E.B. Maiga, C.T. Nguyen, N. Galanis, G. Roy, T. Mare, M. Coqueux, Heat transfer enhancement in turbulent tube flow using Al_2O_3 nanoparticles suspension, Int. J. Numer. Method. H. 16 (3) (2006) 275–292.

[31] P. Hajela, C.Y. Lin, Genetic search strategies in multicriterion optimal design, Struct. Optimization 4(2) (1992) 99–107.

[32] N. Srinivas, K. Deb, Multiobjective optimization using nondominated sorting in genetic algorithms, Evolutionary Computation 2(3) (1994) 221-248.

[33] E. Zitzler, L. Thiele, Multiobjective evolutionary algorithms: a comparative case study and the strength Pareto approach, IEEE T. Evolut. Comput. 3(4) (1999) 257–271.

[34] J.D. Knowles, D.W. Corne, Approximating the nondominated front using the Pareto archived evolution strategy, Evolutionary Computation 8(2) (2000) 149–172.

[35] R. Sarker, K.H. Liang, C. Newton, A new multiobjective evolutionary algorithm, Eur. J. Oper. Res. 140(1) (2002) 12-23.

[36] G.G. Yen, H. Lu, Dynamic multiobjective evolutionary algorithm: adaptive cell-based rank and density estimation, IEEE T. Evolut. Comput. 7(3) (2003) 253–274.

[37] H. Lu, G.G. Yen, Rank-density-based multiobjective genetic algorithm and benchmark test function study, IEEE T. Evolut. Comput. 7(4) (2003) 325–343.

[38] M. Hamdan, A dynamic polynomial mutation for evolutionary multi-objective optimization algorithms, Int. J. Artif. Intell. T. 20(1) (2011) 209–219.

Figure captions

Fig. 1 Structure of the GA-PNN hybrid system for the Nusselt number of TiO_2-water nanofluid modelling

Fig. 2 Structure of the GA-PNN hybrid system for pressure drop of TiO_2-water nanofluid modelling

Fig. 3 Comparison of the experimental data of Sajadi and Kazemi [6] with the GA-PNN proposed model for the Nusselt number and existing correlations (TiO_2-water nanofluid, with an average particle size of 30 nm at a volume concentration of 0.1%)

Fig. 4 Comparison of the experimental data of Duangthongsuk and Wongwises [5] with the GA-PNN proposed model for the Nusselt number and existing correlations (TiO_2-water nanofluid, with an average particle size of 21 nm at a volume concentration of 1%)

Fig. 5 Comparison of the experimental data of Abbasian Arani and Amani [13] with the GA-PNN proposed model for the Nusselt number and existing correlations (TiO_2-water nanofluid, with an average particle size of 50 nm at a volume concentration of 1%)

Fig. 6 Comparison of the experimental data of Abbasian Arani and Amani [13] with the GA-PNN proposed model for the Nusselt number and existing correlations (TiO_2-water nanofluid, with an average particle size of 10 nm at a volume concentration of 1.5%)

Fig. 7 Comparison of the experimental data of Abbasian Arani and Amani [13] with the GA-PNN proposed model for the Nusselt number and existing correlations (TiO_2-water nanofluid, with an average particle size of 20 nm at a volume concentration of 2%)

Fig. 8 Comparison of the experimental data [6, 5 and 13] with the GA-PNN proposed model for pressure drop (***a***-TiO_2-water nanofluid, with an average particle size of 30 nm at a volume concentration of 0.15% [6] ***b***-TiO_2-water nanofluid, with an average particle size of 21 nm at a volume concentration of 1.5% [5] ***c***-TiO_2-water nanofluid, with an average particle size of 30 nm at a volume concentration of 1% [13] ***d***-TiO_2-water nanofluid, with an average particle size of 50 nm at a volume concentration of 1.5% [13])

Fig. 9 Multi-objective Pareto front of the Nusselt number and pressure drop

Table 1

Statistical criteria used for the analysis of the results

Statistical criterion	Equation
Mean absolute error	$MAE = \frac{1}{n}\sum_{i=1}^{n}\left\|X_p - X_a\right\|$
Mean relative error	$MRE(\%) = \frac{100}{n}\sum_{i=1}^{n}\left(\frac{\left\|X_p - X_a\right\|}{X_a}\right)$
Root mean square error	$RMSE = \sqrt{\frac{1}{n}\sum_{i=1}^{n}\left(X_p - X_a\right)^2}$

Table 2

The value of design variables (input variables) and objective functions of the start and end section points

Points	ϕ (%)	d_p (nm)	*Re*	*Pr*	*Nu*	ΔP (kPa)
A	1.93	50	6010	3.19	64.234	2.422
B	1.68	40	8768	4.12	93.106	2.754
C	1.52	35	10143	4.31	106.666	3.284
D	1.31	20	30857	3.5	297.864	12.199
E	1.28	20	32238	3.47	307.299	12.99
F	1.15	20	35120	3.72	313.878	15.521

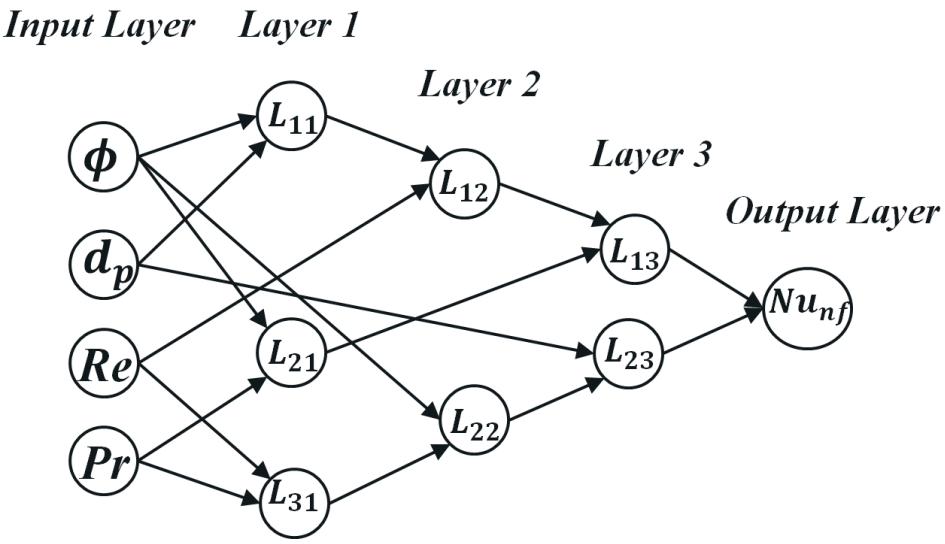
Input Layer
Layer 1
Layer 2
Layer 3
Output Layer
ϕ
d_p
Re
Pr
L_{11}
L_{12}
L_{13}
L_{21}
L_{22}
L_{23}
L_{31}
Nu_{nf}

Fig. 1

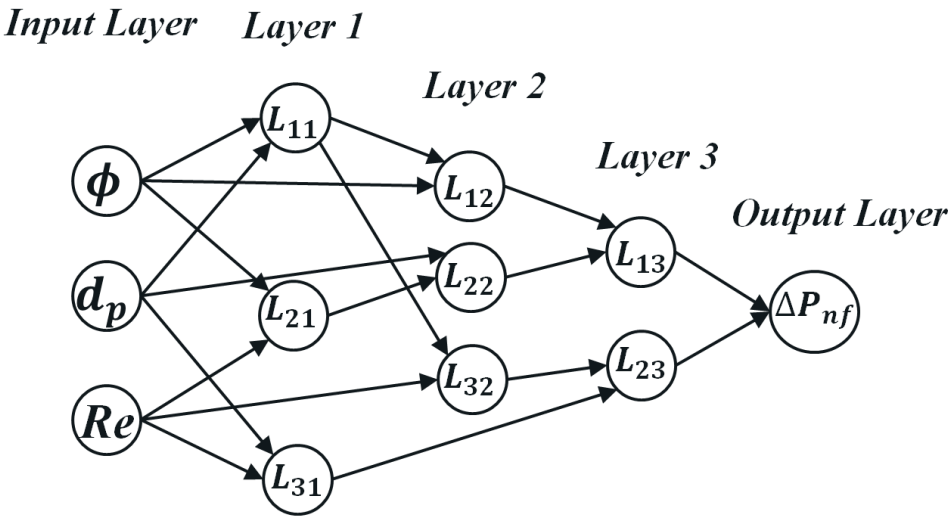
Input Layer
Layer 1
Layer 2
Layer 3
Output Layer
ϕ
d_p
Re
L_{11}
L_{12}
L_{21}
L_{22}
L_{31}
L_{32}
L_{13}
L_{23}
ΔP_{nf}

Fig. 2

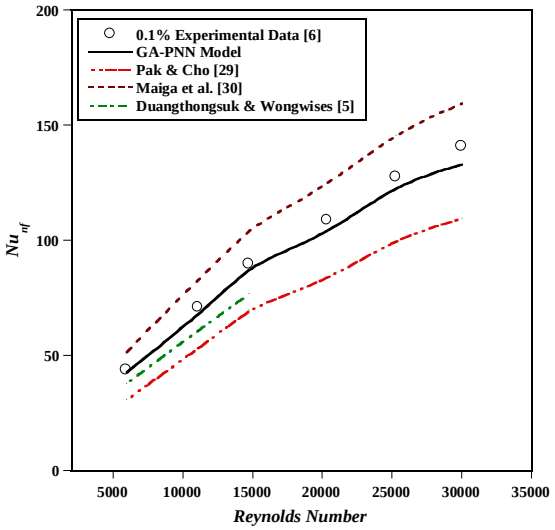
0.1% Experimental Data [6]
GA-PNN Model
Pak & Cho [29]
Maiga et al. [30]
Duangthongsuk & Wongwises [5]
Nu nf
Reynolds Number
200
150
100
50
0
5000
10000
15000
20000
25000
30000
35000

Fig.3

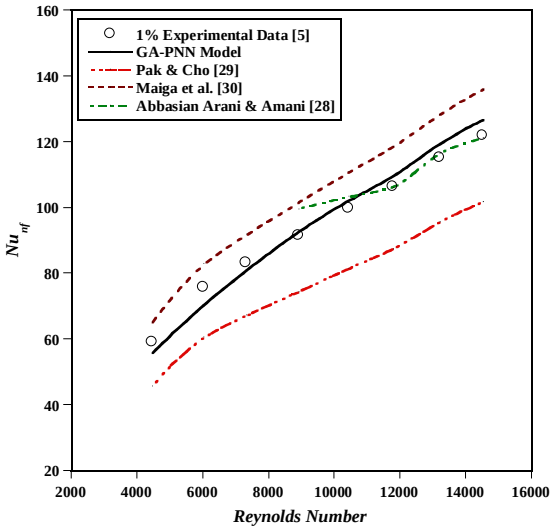
1% Experimental Data [5]
GA-PNN Model
Pak & Cho [29]
Maiga et al. [30]
Abbasian Arani & Amani [28]
Nu nf
Reynolds Number
160
140
120
100
80
60
40
20
2000
4000
6000
8000
10000
12000
14000
16000

Fig.4

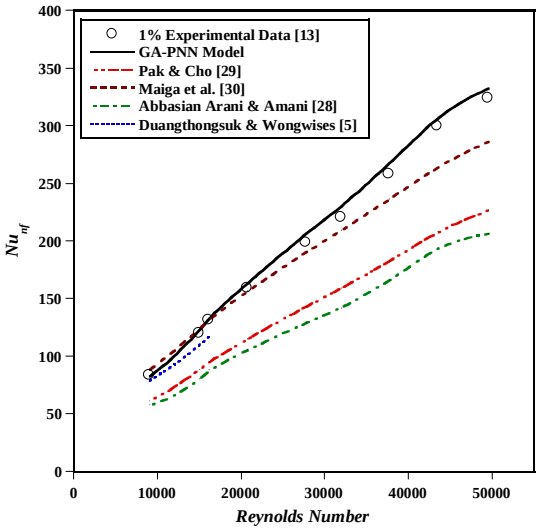
1% Experimental Data [13]
GA-PNN Model
Pak & Cho [29]
Maiga et al. [30]
Abbasian Arani & Amani [28]
Duangthongsuk & Wongwises [5]
Nu_nf
Reynolds Number
0
50
100
150
200
250
300
350
400
0
10000
20000
30000
40000
50000

Fig.5

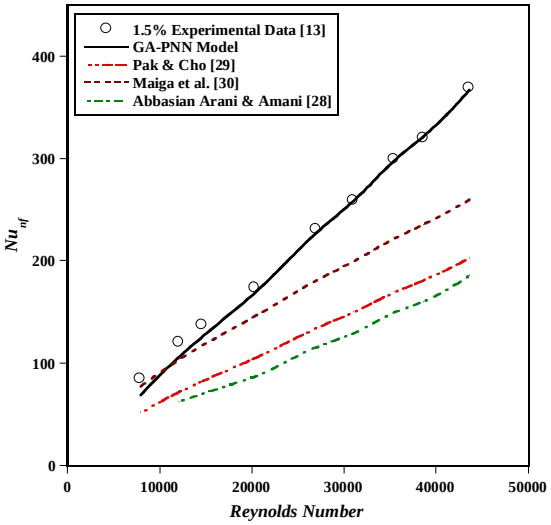
1.5% Experimental Data [13]
GA-PNN Model
Pak & Cho [29]
Maiga et al. [30]
Abbasian Arani & Amani [28]
Nu nf
Reynolds Number
0
100
200
300
400
0
10000
20000
30000
40000
50000

Fig.6

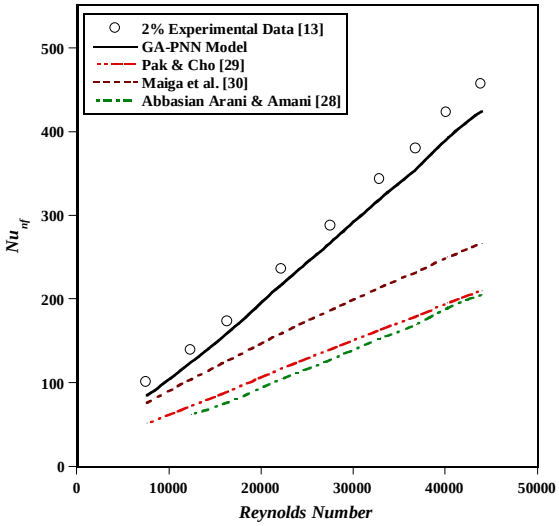
2% Experimental Data [13]
GA-PNN Model
Pak & Cho [29]
Maiga et al. [30]
Abbasian Arani & Amani [28]
Nu_{nf}
0
100
200
300
400
500
0
10000
20000
30000
40000
50000
Reynolds Number

Fig.7

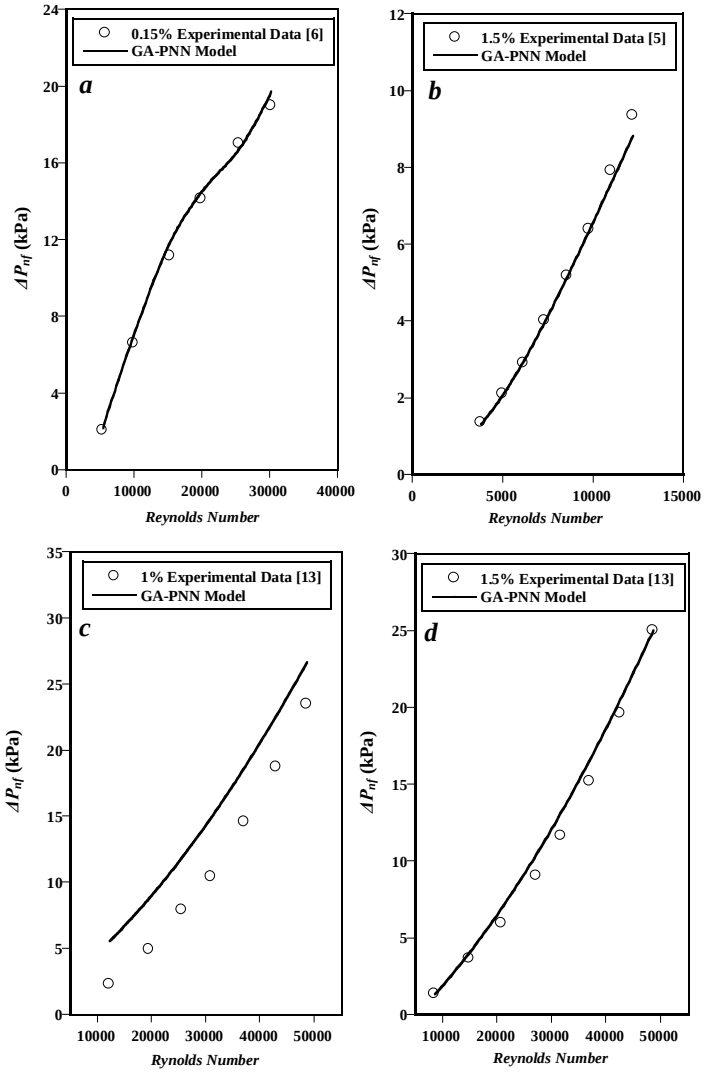
0.15% Experimental Data [6]
GA-PNN Model
a
ΔPnf (kPa)
Reynolds Number
1.5% Experimental Data [5]
GA-PNN Model
b
ΔPnf (kPa)
Reynolds Number
1% Experimental Data [13]
GA-PNN Model
c
ΔPnf (kPa)
Rynolds Number
1.5% Experimental Data [13]
GA-PNN Model
d
ΔPnf (kPa)
Reynolds Number

Fig.8

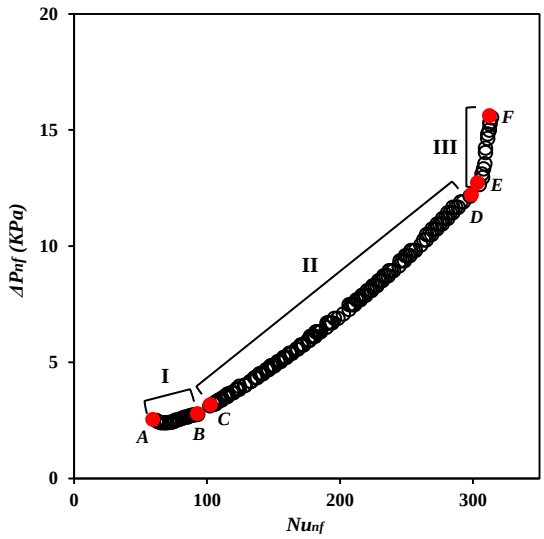

Fig.9